Impurity effect of Mg on the generalized planar fault energy of Al

Dongdong Zhao[a], Ole Martin Løvvik[b,], Knut Marthinsen[a], and Yanjun Li[*,a]

[a]*Department of Materials Science and Engineering, Norwegian University of Science and Technology, 7491 Trondheim, Norway*

[b]*SINTEF Materials and Chemistry, 0314 Oslo, Norway*

*Corresponding author. E-mail: yanjun.li@ntnu.no Tel.: +47 73551206

Abstract

Generalized Planar Fault Energy (GPFE) curves are widely used to evaluate the deformation behavior of metals and alloys. In the present work, a systematic analysis of the microscopic plastic deformation mechanism of face-centered cubic Al in comparison to Cu was conducted based on GPFE curves generated via first-principles calculations. Focus has been put on the effects of Mg impurities in terms of local concentration and local atomic arrangement nearby the deformation plane, upon the GPFE curve of Al, with the aim to investigate the twinnability of Al-Mg alloys subjected to plastic deformation. It is found that Mg exhibites a Suzuki segregation feature to the stacking fault of Al, either intrinsic or extrinsic. Mg atoms residing in the stacking fault plane can decrease the intrinsic stacking fault energy γ_{ISFE} and enhance the twinning propensity of Al. However, the γ_{ISFE} value does not decrease monotonically with increasing Mg concentration in the alloy, and a continuous twinnability increase with increasing Mg content is not observed. It is also seen that different local concentrations and atomic configurations of Mg atoms in the vicinity of deformation plane could yield a large variation of γ_{ISFE} and the twinning propensity of Al. It is proposed that Mg alloying cannot substantially enhance the twinning propensity of Al alloys.

Keywords: Generalized Planar Fault Energy (GPFE), γ_{ISFE}, Suzuki segregation, twinnability, Al-Mg alloys

1. Introduction

With a good combination of formability, high specific strength, weldability and corrosion resistance, aluminium alloys are widely applied in transportation sectors. In order to further increase the strength of aluminium alloys, various severe plastic deformation (SPD) strategies such as equal channel angular pressing (ECAP) [1, 2], high pressure torsion (HPT) [3, 4], dynamic plastic deformation (DPD) [5] have been applied to attain ultra-fine-grained (UFG) or even nano crystalline structures. Nevertheless, most of the UFG or nano structured metals and alloys processed by SPD methods possess poor ductility. It has been found that the nano twin structures can significantly increase the strength without sacrificing the ductility of metals, e.g. Cu alloys [6, 7]. However, deformation twinning is difficult to occur in coarse grained Al alloys during plastic deformation. This has been attributed to the high intrinsic stacking fault energy γ_{ISFE} and a high ratio between unstable twinning fault energy γ_{UTFE} and unstable stacking fault energy γ_{USFE}. Promisingly, Mg has been reported to be a potential alloying element to reduce γ_{ISFE} in Al [8]. By using the Layer Korringa Kohn Rostoker methodology, Schulthess et al. [9] calculated the γ_{ISFE} of disordered Al-Mg alloys and showed a nearly linear decrease of γ_{ISFE} with increasing Mg content (below 40 at.% Mg). Though different in quantity, the γ_{ISFE} values of different Al-Mg alloys, determined by different experimental methods also showed that γ_{ISFE} decreases significantly with increasing Mg content in the alloys, e.g. for a Al–3.59 at.% Mg alloy, γ_{ISFE} has been determined as low as 54 mJ/m^2 [10], which is even comparable to that of pure Cu. By fitting the experimentally determined γ_{ISFE} values, Morishige et al. [10], proposed an empirical equation to address the Mg concentration effect on γ_{ISFE} in Al-Mg alloys.

$$\gamma_{Al-Mg} = \gamma_0 \cdot \exp\left\{ k_\gamma \left(\frac{x_{Mg} / x^*_{Mg}}{1 + \left(x_{Mg} / x^*_{Mg} \right)} \right)^2 \right\} \qquad \text{Eq. (1)}$$

where x^*_{Mg} denotes the solubility limit of Mg in Al matrix, k_γ is a dimensionless constant, and γ_0 signifies the stacking fault energy in pure Al. This equation predicts a further reduced γ_{ISFE} at a Mg concentration of 5.30 at.% to 29.2 mJ/m^2. With the low γ_{ISFE} character, Al-Mg alloys with high Mg contents do exhibit some special deformations behaviors. For instance, unlike the wavy glide in pure Al and most other Al alloys, Al-Mg alloys show a planar glide behavior [11, 12] during plastic deformation. By the high strain rate DPD technique, a significant fraction of incoherent twin boundaries could be generated in a coarse grained Al-7 wt.% Mg alloy [13]. However, coherent deformation twins have rarely been observed in Al-Mg alloys, except for under some extreme conditions. For instance, Gray [14] observed deformation twinning in Al–4.8 wt.% Mg alloy subjected to shock loading (strain rate ~10^7 s^{-1}) at a low temperature of -180°C. Then a question arises: can Mg addition dramatically decrease γ_{ISFE} and therefore make twinning the dominant deformation

mechanism in Al-Mg alloys? Due to the difficulty in accurate determination of γ_{ISFE} through experiments [15], further investigation with more reliable methods are needed to calculate the Mg concentration effect on γ_{ISFE} of Al-Mg alloys.

Fortunately, we can turn to first-principles calculations which were proved to be a powerful tool in many research fields [16, 17], to accurately quantify this material parameter based on the concept of Generalized Planar Fault Energy (GPFE), firstly put forward in 1970s by Vítek [18], which actually represents the energy penalty per area induced by the rigid shift of two parts of the crystal via the displacement vector ***f*** [19]. To be specific, ***f*** is mostly set along the <112> direction in {111} slip planes for *fcc* metals. Four typical energy points would be encountered along the GPFE displacement path, with the first three extremal points indicating γ_{USFE}, γ_{ISFE}, γ_{UTFE}, and the last point as the twinning fault (two-layer micro twin) energy γ_{TFE}, which is also interpreted as the extrinsic stacking fault energy γ_{ESFE} [20]. Extensive efforts have been dedicated to the investigation of GPFE curves to probe the propensity for formation of dislocations, twinning nucleation, as well as the deformation mechanisms in nano crystalline (nc) materials, eg. nc Al, Ni and Cu [8, 19-38]. It is showed that γ_{ISFE} alone is not a fully adequate parameter to evaluate the twinnability of metals and alloys. Particularly, the incorporation of GPFE curves with analytical models can help to comprehend and predict many experimental phenomena associated with dislocations, such as Peierls stress [21, 22], deformation twinning stress [26, 37] and plastic deformation regimes [20, 38] etc. All these works validate the high efficiency of GPFE in describing nucleation, formation of dislocations, as well as the competition between different deformation regimes.

Using GPFE calculated by Density Functional Theory (DFT), Muzyk et al. [8] predicted a reduced γ_{ISFE} and $\gamma_{UTFE}/\gamma_{USFE}$ with one Mg atom substituting an Al atom at the deformation plane in a 48-atom Al matrix, thus concluded that Mg alloying can promote twinning in Al. However, a more detailed investigation of the Mg concentration effect on GPFE in Al-Mg alloys is missing. A systematic study on the effect of the concentration and the local arrangement of Mg atoms in the vicinity of the deformation plane on the twinning tendency of Al-Mg alloys is also needed. In light of the above considerations, first-principles calculations are thus initiated with the aim to investigate the impurity effect of Mg on the GPFE of Al, so as to probe the twinnability and deformation behavior of Al-Mg alloys.

2. Computational methodology

All the calculations in the present work were performed based on the first-principles plane wave pseudopotential method as implemented in the highly-efficient Vienna ab initio simulation package (VASP) [39, 40]. Electron–ion interactions were treated with the full potential frozen-core

projector augmented wave (PAW) method [41, 42]. The Generalized Gradient Approximation (GGA) of Perdew–Burke–Ernzerhof (PBE) [43] was selected to describe the exchange–correlation functions. A cutoff of 350 eV was employed in all the calculations to insure the total energy differences were less than 1 meV/atom. Following the Monkhorst-Pack scheme [44], a *k*-points sampling of 13×7×1 together with the linear tetrahedron method including Blöchl corrections [45] was adopted for the reciprocal-space energy integration in the Brillouin zone (BZ). The convergence criteria of 10^{-6} eV and 10^{-4} eV/Å were employed for electronic self-consistency and ionic loop, respectively, in the relaxation process.

To find the energetically favorable distributions of Mg in the Al matrix, a 48-atom supercell as illustrated in Fig. 1(a) was adopted to investigate the binding energy of Mg-Mg pairs in the Al matrix. By setting Mg at different positions (see Fig. 1(a) and Table 1) for substitution, the binding energies of Mg-Mg pairs at different neighboring state can be evaluated in terms of the following equation:

$$E_b\left(X-X\right)=-\left(E_{(Al_{46}X_2)}+E_{(Al_{48})}-2E_{(Al_{47}X_1)}\right) \qquad \text{Eq. (2)}$$

Specifically, $E_{(Al_{46}X_2)}$, $E_{(Al_{47}X_1)}$, $E_{(Al_{48})}$ are DFT total energies of the supercell with two Mg atoms at different neighboring positions, with one Mg impurity, and without any defects, respectively. Note that a positive E_b value indicates attractive interaction of the pair. Table 1 lists the predicted E_b of Mg-Mg pairs at different neighboring distances in the Al matrix. It shows that E_b of 2nd nearest neighbor (2nn, 2nn') and 4th nearest neighbor (4nn, 4nn') have significantly higher values than the other arrangements, suggesting that Mg atoms prefer to form clusters with two atoms locating at the second or fourth nearest neighbor lattice site of each other. This binding feature is similar to what was found previously for Si and Mn solutes in Al [46].

In the calculation of GPFE curve, a perfect stacking sequence of 12 (111) planes (ABCABCABCABC) containing 96 atoms was constructed. A slab model containing a vacuum spacing of 15 Å along the <111> direction as shown in Fig. 1(b) was established to inhibit the interactions between stacking faults. Energies were calculated for different configurations obtained by displacing half of the crystal in reference to the other along the $<1\bar{1}2>$ direction within (111) planes (see Fig. 1(b)). To obtain the whole GPFE curve, two separate displacing operations of the slab model along the $<1\bar{1}2>$ direction had to be enforced. In each operation, the final displacement distance was the Burgers vector of a partial dislocation, which is $a_0/\sqrt{6}$, with a_0 as the lattice constant of the Al crystal. In the first displacing step, layers numbered as 1–6 in one-half of the crystal were displaced to form a stacking fault. In the second, based on the previously formed stacking fault configuration, layers numbered from -1 to -5 in the lower part of the crystal were displaced in the opposite direction. A conjugate-gradient relaxation algorithm was adopted to attain the equilibrium state of different

configurations. The atomic positions were selectively allowed to relax in the direction perpendicular to the stacking fault plane. Energies of the different configurations along the GPFE curve were calculated using Eq. (3) [47]:

$$E\left(\vec{f}\right)=\frac{E_{faulted}\left(\vec{f}\right)-E_{perfect}}{A} \quad , \qquad \text{Eq. (3)}$$

in which $E_{faulted}\left(\vec{f}\right)$ is the total energy of the supercell with a fault vector $\vec{f}$, $E_{perfect}$ represents the total energy of the perfect stacking slab, and A is the area of the fault plane.

3. Results and discussion

3.1 GPFE curves of Al in comparison to Cu

Table 2 collects the calculated values of GPFE in the present work, including γ_{USFE}, γ_{ISFE}, γ_{UTFE}, and γ_{TFE} of Al, as well as $\gamma_{ISFE}/\gamma_{USFE}$, $\gamma_{UTFE}/\gamma_{USFE}$ and γ_{UTFE}-γ_{USFE}, in comparison with previous calculation and experimental results. As indicated in Table 2, the experimentally determined values of γ_{ISFE} are scattered and vary widely from 135 to 200 mJ/m^2, due to the limited accuracy of experimental methods [48]. γ_{ISFE} for Al evaluated from first-principles calculations shows a more narrow range, varying from 122 to 164.2 mJ/m^2. In general, three first-principles based approaches have been adopted to evaluate γ_{ISFE}, (i) direct approach, which is the direct estimation of the energy penalty between the perfect stacking and the stacking fault structures; (ii) slab shear deformation, a commonly used approach to determine the GPFE, which is enforced via the rigid relative displacement of two parts of a slab configuration; (iii) alias shear deformation, including pure alias shear and simple alias shear, originally proposed by Jahnátek [29]. Different approaches may provide slightly different γ_{ISFE}. Besides, the different pseudopotentials as used in the calculations (cf. Table 2) could be another reason to account for the variation of γ_{ISFE} for Al obtained by first-principles approaches. Other methodologies for calculating γ_{ISFE} or even GPFE include Molecular Dynamics (MD) [20], (Modified) Embedded Atom Method ((M)EAM) [33], Tight Binding (TB) [49] etc. These methods have predicted a larger variety range of γ_{ISFE} of Al, from 95.4 to 170.0 mJ/m^2. It is worth noting that GPFE evaluated by MD and (M)EAM strongly depends on the atomic potentials used in the simulations. The as-predicted γ_{ISFE} of Al, 142.4 mJ/m^2 in the present work, is close to the average of values from first-principles calculations. This quantity identifies Al as a high stacking fault energy (SFE) material. We found excellent agreement between the present work and that of Hunter [36], who used the same approach and pseudopotential as in the present work.

Turning to Cu, the GPFE obtained in the present work together with previous theoretical and experimental results are summarized in Table 3, the parameters $\gamma_{ISFE}/\gamma_{USFE}$, $\gamma_{UTFE}/\gamma_{USFE}$, and γ_{UTFE}-γ_{USFE} are also included. Experimentally determined values of γ_{ISFE} lies in the range of 42-78 mJ/m^2, exhibiting a much smaller variation than that of Al. The present work yields a calculated value of 40.5 mJ/m^2 for γ_{ISFE}, which is close to the median value of the determined γ_{ISFE} via first-principles calculations, varying from 33.0 to 50.0 mJ/m^2. This classifies Cu as a low SFE material. γ_{ISFE} of Cu evaluated via other methodologies including MD [20], (M)EAM [33], Morse Potential [50] etc. yield values between 20.6 to 70.8 mJ/m^2, again bearing a large variation. As indicated in Table 3, best agreement can be found between present work and the results by Asadi et al. [33] and Hunter [36]. It is worth noting that one should be careful with direct comparison between the GPFE from first-principles calculations and experiments, since experimental measurements are usually carried out at room temperature while first-principles calculations refer to 0 K.

The GPFE curve in *fcc* metals characterizes the energy penalty to displace the (111) planes relative to neighboring (111) planes along the $<1\bar{1}2>$ direction. Many works done before confirm that γ_{ISFE} alone is not sufficient to understand the underlying mechanisms of deformation processes [20, 38]. Instead, several features of the full GPFE curves are needed to determine the plastic deformation mechanisms of materials, and to predict the propensity for formation of stacking faults, nucleation of dislocations and deformation twins. It is generally believed that three distinct deformation mechanisms exist in *fcc* metals: twinning (TW), stacking faults (SF), and full slip (FS) [38]. To compare the deformation mechanism in Al and Cu, their GPFE curves, including TW, SF and FS, are shown in Fig. 2(a) and (b), respectively. The first extremal point along the GPFE curves of Al and Cu indicates γ_{USFE}, i.e. the energy barrier which has to be overcome to nucleate a leading partial dislocation (usually from a grain boundary). An intrinsic stacking fault will be left behind after the nucleation of leading partial dislocation. The second energy extremal point defines the intrinsic stacking fault energy γ_{ISFE}. After the nucleation of a leading partial dislocation, a competition exists between the three possible deformation mechanisms. The pre-deformed crystal can nucleate a trailing partial dislocation to form a full dissociated dislocation (FS), or nucleate a twin partial dislocation in an adjacent plane to form a two-layer micro twin (TW), or nucleate another leading partial dislocation in a non-adjacent plane to form another stacking fault (SF), which is actually the successive generation of stacking faults. The third energy extremal point along the TW deformation mode is interpreted as γ_{UTFE}, corresponding to the energy barrier to nucleate a twinning partial dislocation. After the nucleation of twinning partial dislocation, a two-layer micro-twin or equivalently an extrinsic stacking fault will be created, of which the configuration energy is identified as γ_{TFE} or γ_{ESFE}, correspondingly.

In recent years, different parameters have been proposed to predict the predominant deformation mechanism especially twinability in metals, based on GPFE. Rice [51], Tadmor and Hai [52] developed important criteria which have been widely accepted and employed to evaluate the deformation mechanism competition between FS and TW, based on $\gamma_{ISFE}/\gamma_{USFE}$ and $\gamma_{UTFE}/\gamma_{USFE}$. A deformation mechanism by FS is more energetically favorable if the values of $\gamma_{ISFE}/\gamma_{USFE}$ are close to unity; on the contrary, when these parameters are far from unity, formation of partial dislocations and twins would be expected. In addition, Tadmor and Bernstein [53, 54] proposed another approximate criterion to evaluate the twinnability, which quantifies the propensity of *fcc* metals to undergo deformation twinning based on the number and strength of active twinning systems in terms of γ_{USFE}, γ_{ISFE} and γ_{UTFE}:

$$\tau_a = \left[1.136 - 0.151\frac{\gamma_{ISFE}}{\gamma_{USFE}}\right]\sqrt{\frac{\gamma_{USFE}}{\gamma_{UTFE}}} \qquad \text{Eq. (4)}$$

A larger τ_α indicates an increased tendency for twinning. A simpler expression to evaluate twinnability is $\delta = \gamma_{UTFE}-\gamma_{USFE}$, i.e. a smaller δ means increased susceptibility for twinning.

Based on the GPFE of Al and Cu and the above criteria, it is possible to analyze the competition between FS, TW, and SF in Al and Cu. As can be seen in Fig. 2(a) and (b), it is difficult to activate the SF deformation regime in both Al and Cu, since the energy barrier is higher for SF formation than that of FS and TW. It follows in Table 2 and 3 that Cu has a much smaller $\gamma_{ISFE}/\gamma_{USFE}$ value than Al, and therefore has a larger tendency to nucleate leading partial dislocations during deformation. A negative correlation should be expected for $\gamma_{UTFE}/\gamma_{USFE}$ and τ_a, since a high propensity for deformation twinning is characterized by a large (small) τ_a ($\gamma_{UTFE}/\gamma_{USFE}$). Indeed, this is exactly what is seen in the case of Cu. Along the GPFE curves of Al and Cu in Fig. 2(a) and (b) it is evident that after the nucleation of a leading partial dislocation it is much easier for Al to emit a trailing partial dislocation to form a complete perfect dislocation, thus entering the 'perfect dislocation' - FS deformation regime. A higher value of $\gamma_{UTFE}-\gamma_{USFE}$ for Al means a larger energy barrier for twin nucleation, which hinders the pre-existing stacking fault configurations to enter the twinning deformation regime. Cu is on the other hand displaying a much smaller $\gamma_{UTFE}-\gamma_{USFE}$, so that deformation twinning is much more energetically probable. Recently, Jo et al. [38] proposed the intrinsic slip barrier, defined as $\gamma_d=\gamma_{ISFE}/(\gamma_{USFE}-\gamma_{ISFE})$, to classify the deformation characteristics of materials. For *fcc* metals having $0<\gamma_d<2$, both twinning and FS can be activated during plastic deformation, while for metals possessing $\gamma_d>2$, deformation will be governed by FS. Based on the GPFE obtained in the present work, we obtain a γ_d value of 0.335 for Cu, implying a combined deformation regime of TW

and FS. While the corresponding value for Al, is γ_d=4.07, which means that FS will be the dominant deformation mechanism – all consistent with the analysis based on τ_a and $\gamma_{UTFE}/\gamma_{USFE}$.

3.2 Effect of Mg alloying on GPFE of Al and Suzuki segregation of Mg in Al

In order to evaluate the effect of solute Mg on the GPFE curve of Al, we substituted one Al atom with a Mg atom in the stacking fault plane (layer 0 in Fig. 1(b), site 1 in Fig. 1(c)) in a supercell containing 96 atoms ($Al_{95}Mg_1$). This implies an overall Mg concentration of 1.08 at.% and layer concentration of 12.5 at.%. The effect of this single Mg solute on γ_{USFE}, γ_{ISFE}, γ_{UTFE}, and γ_{TFE} values of Al are summarized in Table 4, and the corresponding GPFE curve of Al is shown in Fig. 3. It follows that the introduction of Mg impurity not only decreases γ_{ISFE} of Al, i.e. from 142.4 mJ/m^2 to 135.0 mJ/m^2, but also reduces the other three extremal energy points. This is consistent with previous theoretical calculations [8] and experimental measurement results [55]. Muzyk et al. [8] reported that alloying with Mg would increase the tendency for formation of partial dislocations and twinnability of Al. In the present work, we verified that Mg alloying can promote twinning due to the increased τ_a and decreased $\gamma_{UTFE}/\gamma_{USFE}$, γ_{UTFE}-γ_{USFE}, compared with pure Al (as shown in Table 4). However, we do not see an increased tendency for formation of partial dislocations induced by Mg alloying since it has nearly the same $\gamma_{ISFE}/\gamma_{USFE}$ as pure Al.

In most previous simulation works evaluating the alloying effect of GPFE, the solute atoms are placed in the stacking fault plane. This is based on the Suzuki segregation, a well-known phenomenon of impurity solutes segregating towards stacking faults. However, the detailed mutual interactions between solutes at different layers and stacking faults are scarcely considered. It has been revealed recently that the Suzuki effect is not a universal phenomenon for any elements and some solute elements even exhibit anti-Suzuki segregation characteristics in some alloy systems [56]. Actually the Suzuki segregation is practically determined by the interaction energy between stacking faults and solute atoms, which is defined as the energy difference between the stacking fault configuration when a solute atom resides in the *n*th atomic layer from the fault plane and the pure stacking fault configuration. This interaction energy can be evaluated based on the following equation [57]:

$$E_{\text{int}}^{n} = \left(E_{SF}^{Sol-n} - E_{PS}^{Sol-n}\right) - \left(E_{SF} - E_{PS}\right) \qquad \text{Eq. (5)}$$

Here, E_{SF}^{Sol-n} is the total energy of the stacking fault with the solute atom residing in the *n*th atomic layer from the fault plane. E_{PS}^{Sol-n} is the energy of a model with perfect stacking and one solute atom. E_{SF} and E_{PS} are the total energies of the stacking fault and perfect stacking configurations without solute atoms. It is interesting to note that E_{int}^{n} can also be interpreted as the segregation energy of

solutes to the stacking fault; a negative value of E_{int}^{n} indicates the solute atom will prefer to segregate to the stacking fault. E_{int}^{n} is not limited in the stacking fault plane, and has a spatial distribution in the vicinity of the fault plane. This characteristic energy distribution would lead to the spatial concentration profile of the solutes near the stacking fault defect. The layer by layer equilibrium concentration of solutes in the vicinity of the stacking fault at finite temperature *T* can be predicted from the following equation [58]:

$$c(n) = \frac{1}{1 + \frac{1 - c_0}{c_0} \exp\left(\frac{E_{\text{int}}^{n}}{k_B T}\right)} \qquad \text{Eq. (6)}$$

Here, $c(n)$ is the solute concentration in the *n*th atomic layer. c_0 is the nominal concentration far from the stacking fault, k_B is the Boltzmann constant.

To get insight into the Suzuki effect of Mg in Al, the layer by layer interaction E_{int}^{n} between Mg and intrinsic as well as extrinsic stacking fault are calculated and the results are presented in Fig. 4(a), with layers numbered according to the labelling in Fig. 1(b). It can be seen that E_{int}^{n} only extends a couple of atomic layers away from the stacking fault plane, i.e. two layers for intrinsic stacking fault, three layers for extrinsic stacking fault, and diminishes at longer distances. A negative E_{int}^{n} at the stacking fault plane indicates that Mg is attracted to stacking fault, either intrinsic or extrinsic, exhibiting a Suzuki segregation feature. The more negative the E_{int}^{n} value is, the higher tendency is for Suzuki segregation. Furthermore, the interaction is stronger between Mg and the extrinsic stacking fault than the intrinsic stacking fault, suggesting a stronger segregation tendency of Mg towards the former. A small energy barrier can also be seen at layers -2 and 3 for intrinsic stacking fault in Fig. 4(a), revealing a slightly activated Suzuki segregation feature [56]. In addition to the energies barriers indicated in Fig. 4(a) (which only present energies of Mg residing on stable lattice sites), diffusion towards the stacking fault would also involve overcoming the activation energy of transition states in vacancy mediated diffusion [59]. This was implemented through a diffusive molecular dynamics technique based on the embedded-atom method by Dontsova et al. [58], which yielded results in reasonable correspondence with the present work. It is interesting to see that the effective barrier for Suzuki segregation of Mg towards the extrinsic stacking fault is relatively large, due to the large energy barriers involved in moving from layers -2 and 2 to layers -1 and 1, respectively, as shown in Fig. 4(a). This suggests the difficulty for Mg to diffuse/segregate to extrinsic stacking fault than to the intrinsic to alter their energy state, due to the larger kinetic barrier.

Figure 4(b) presents the spatial equilibrium concentration profile of Mg near the stacking fault as evaluated from Eq. (6) with a nominal concentration of c_0 = 1% and room temperature T = 300 K. Local enrichment of Mg at the stacking fault region induced by Suzuki segregation is observed both for intrinsic and extrinsic stacking faults. As for the intrinsic stacking fault, the atomic layers representing the fault planes (layers 0 and 1 in Fig. 1(b)) have the highest concentration of Mg. A slightly decreased concentration of Mg can be seen at the planes adjacent to the fault plane. This behavior is in good agreement with the enrichment of Mg near the intrinsic stacking fault simulated by Dontsova et al. [58]. When we turn to the extrinsic stacking fault, an oscillatory concentration distribution with three peak concentrations of Mg near the stacking fault region is observed. It is worth noting that Eq. (6) is only valid at low c_0, since solute-solute interactions would be decisive for the local Mg distribution at high c_0.

3.3 Effects of varying Mg concentrations on the GPFE curve of Al

To study the dependence of the GPFE of Al on the Mg concentration, different numbers of Mg atoms were introduced to substitute Al atoms in the Al slab matrix. Several different configurations were introduced, based on the binding energies between Mg atoms in Al (see Table 1) and the fact that the Mg-stacking fault interaction only extends a couple of atomic layers from the fault plane. Complete layer substitution of Mg solutes was avoided, since repulsive interactions encourage the Mg atoms to be spatially distributed, as evidenced in the previous section. Moreover, to avoid an asymmetrical impact on the GPFE, we kept the Mg atoms symmetrically distributing in the vicinity of deformation plane. We considered one model with 2 Mg solute atoms ($Al_{94}Mg_2$), four with 3 ($Al_{93}Mg_3$), two with 4 ($Al_{92}Mg_4$) and four models with 6 solute atoms ($Al_{90}Mg_6$). These models correspond to an overall concentration of 2.08 at.%, 3.13 at.%, 4.17 at.% and 6.25 at.% Mg, respectively, in bulk Al. The detailed Mg atomic occupations of these configurations are summarized in Table 4 with occupation numbers referring to Fig. 1(c).

The obtained GPFE values from these simulations are listed in Table 4, and the corresponding GPFE curves are presented in Fig. 5. Apparently, for the $Al_{94}Mg_2$ model with two Mg in the deformation plane, γ_{ISFE} is further reduced from 135.0 for $Al_{95}Mg_1$ to 130.9 mJ/m^2. A further decrease of γ_{USFE}, γ_{UTFE}, and γ_{TFE} was also observed. Still, based on $\gamma_{ISFE}/\gamma_{USFE}$, no increased tendency for formation of partial dislocations is predicted at this Mg concentration. However, a slightly increased τ_a indicates that $Al_{94}Mg_2$ possesses a higher propensity to undergo deformation twinning than $Al_{95}Mg_1$. This may suggest that as more Mg segregate to the stacking fault plane, γ_{ISFE} is further reduced and an increased tendency of twinning can be expected.

When the nominal Mg concentration was increased to 3.13 at.%, four different configurations were adopted. In the $Al_{93}Mg_3$-1 and $Al_{93}Mg_3$-2 configurations, one Mg was positioned in the center of the deformation plane and the other two Mg atoms were residing in layers 2 and -2 as the 4nn, 4nn' of the central Mg atom (see column of "Occupation" in Table 4). A further increased twinning propensity was predicted for $Al_{93}Mg_3$-1, as indicated by the highest τ_a value seen in the present work: 0.919 (see Table 4). Nevertheless, instead of further reduction, a slight increase was observed for γ_{ISFE} in $Al_{93}Mg_3$-1, as will do for γ_{USFE} and γ_{UTFE}. On the other hand, $Al_{93}Mg_3$-2 possesses a comparable τ_a value and twinnability to $Al_{92}Mg_4$-2. Going to $Al_{93}Mg_3$-3 and $Al_{93}Mg_3$-4, three Mg solutes was placed in the three layers near the fault plane, leading to reduced twinnability compared with Al. The lowest value of γ_{ISFE} in the present work was that predicted for $Al_{93}Mg_3$-4, i.e. = 128.4 mJ/m^2.

At the nominal concentration of 4.17 at.%, two configurations, $Al_{92}Mg_4$-1 and $Al_{92}Mg_4$-2 were used. With the deformation plane being occupied with two Mg atoms in $Al_{92}Mg_4$-1, the extra two Mg atoms were set to occupy sites 5 and 7 in layers 1 and -1 (see Fig. 1(c)) as the 2nn and 2nn' to the Mg atoms in the fault plane. In the $Al_{92}Mg_4$-2 model, the extra two Mg atoms were placed in sites 9 and 11 in layers 2 and -2 (Fig. 1b) as 4nn, 4nn' to Mg in the fault plane. As can be seen in Table 4, the reduced γ_{USFE} in $Al_{92}Mg_4$-1 in comparison to that of $Al_{93}Mg_3$, would energetically facilitate the nucleation of leading partial dislocations. However, there is no further decline for γ_{ISFE} at this increased Mg concentration, as compared to the minimum value found for $Al_{93}Mg_3$. The $Al_{92}Mg_4$-1 model exhibits a very low τ_a, even less than pure Al. It also features a relatively high $\gamma_{ISFE}/\gamma_{USFE}$, corresponding to a high probability of entering the FS deformation regime. By contrast, τ_a of $Al_{92}Mg_4$-2 has a surprisingly high value of 0.916 (see Table 4), implying a high propensity of twinning. The different GPFE values of $Al_{92}Mg_4$-1 and $Al_{92}Mg_4$-2 are attributed to the different distributions of Mg solutes in the vicinity of the deformation plane. In addition, we find that Mg solutes residing in layers 1 and -1 adjacent to the deformation plane would reduce twinning probability and thus favor a dislocation-mediated slip deformation regime.

To investigate an even higher Mg concentration effect on the GPFE of Al, four models with a nominal concentration of 6.25 at.% were considered ($Al_{90}Mg_6$-1, $Al_{90}Mg_6$-2, $Al_{90}Mg_6$-3, $Al_{90}Mg_6$-4 as tabulated in Table 4). The results are shown in Fig. 5(e-f) and Table 4. As can be seen, only the $Al_{90}Mg_6$-2 configuration gives a relatively high twinning tendency, τ_a = 0.906, which is still lower than the maximum τ_a values achievable for $Al_{94}Mg_2$, $Al_{93}Mg_3$ and $Al_{92}Mg_4$ configurations. This clearly indicates that the twinnability of Al-Mg alloys does not increase monotonically with increasing Mg content in the alloy. Further reduction in γ_{ISFE} at this rather high Mg concentration was not observed; the lowest value of γ_{ISFE} = 131.8 mJ/m^2 was found for the $Al_{90}Mg_6$-4 model, which is larger than the minimum γ_{ISFE} of $Al_{94}Mg_2$ and $Al_{93}Mg_3$. Furthermore, $Al_{90}Mg_6$-1 has a γ_{ISFE} parameter

that is even higher than that of Al, which is attributed to the pronounced Mg solute repulsion between layer 1 and fault plane. It is worth noting that $Al_{90}Mg_6$-4 has the lowest γ_{USFE} calculated in the present work (cf. Table. 4), which should facilitate nucleation of leading partial dislocations.

4. Discussion

Figure 6 displays the calculated intrinsic stacking fault energy, γ_{ISFE} of Al-Mg alloys with different Mg configurations near the deformation plane, as a function of Mg concentration. It follows in Fig. 6 that nearly all the Al_xMg_y models possess a lower γ_{ISFE} than pure Al (except for $Al_{90}Mg_6$-1), which indicates that Mg alloying can tailor down the γ_{ISFE} of Al, being consistent with the experimental results [55, 60]. However, a linear reduction of γ_{ISFE} with increasing Mg concentration (below 40 at.% Mg) as reported by Schulthess et al. [9] is not observed. As shown in Fig. 6, γ_{ISFE} decreases continuously with increasing Mg content up to 3.13 at.%. When the nominal concentration of Mg is increased to 4.17 at.% and 6.25 at.%, there is a slight increase of γ_{ISFE}. Still, the local concentration and local atomic arrangement of Mg solutes in the vicinity of deformation plane has a strong influence on γ_{ISFE}. A distinct Mg solute atomosphere can produce a considerable variation of γ_{ISFE}. The largest decrease of γ_{ISFE} relative to pure Al was found to be 12 mJ/m^2 for the $Al_{93}Mg_3$-4 model, yet this decrease is far less than the significant decreasing effect upon γ_{ISFE} from Mg solutes as reported by Morishige et al. [10], based on an empirical correspondence between alloy composition, stacking fault energy and grain size of Al-Mg alloys. This reduction of γ_{ISFE} is also much less than that those reported experimental values [55]. Thus it may suggest that Mg alloying is not so effective as expected in the stacking fault energy engineering of Aluminium alloys. This conclusion is shared by Gray [14] that Mg solutes shouldn't drastically decrease the intrinsic stacking fault energy of Al. Furthermore, measurements by Kritzinger [60] also showed that an addition of 0.65 wt.% Mg to Al does not significantly lower γ_{ISFE}.

τ_a and γ_{UTFE}-γ_{USFE} are important parameters in describing the twinnability of metals. Looking at the variation of τ_a versus γ_{UTFE}-γ_{USFE} of Al_xMg_y as displayed in Fig. 7(a), one can find that an inverse-linear relation persists between these two parameters. As an example, the model $Al_{90}Mg_6$-1 with the highest γ_{UTFE}-γ_{USFE} corresponds to the lowest twinnability (τ_a), while $Al_{93}Mg_3$-1 with a low γ_{UTFE}-γ_{USFE} has a high τ_a. It indicates that the higher the γ_{UTFE}-γ_{USFE}, the lower the twinnability parameter of τ_a is, and vice versa. The close correspondence between τ_a and γ_{UTFE}-γ_{USFE} presented in Fig. 7(a) confirms their mutual consistency as predictive parameters for the twinning propensity of *fcc* metals.

The twinnability τ_a of Al_xMg_y models is displayed as a function of Mg concentration in Fig. 7(b). Clearly, a continuously increasing τ_a with the Mg concentration is not observed. As can be seen,

τ_a increases up to the peak value at a Mg content of 3.13 at.%, while it decreases when moving to higher Mg concentrations. Also, it can be noted that not all the Al_xMg_y models possesses higher twinnability than pure Al. Similar to the effect on γ_{ISFE}, the local concentration and local atomic arrangement of Mg solutes near the deformation plane have a strong influence on the twinnability, which consequently, produces several τ_a values even for the same Mg concentration.

Without considering the effect of mutual interactions of Mg solutes at higher concentrations upon the GPFE of Al, Muzyk et al. [8] has predicted that Mg alloying can promote twinning in Al. Nevertheless, we find that though under certain local arrangements, Mg solutes do increase the twinnability of Al. However, the highest increased twinnability found in our study (0.919 for the $Al_{93}Mg_3$-1 model) is still much less than that of pure Cu (τ_a =1.036), which is an indication that the potential of enhancing the twinning tendency of Al by Mg alloying is quite limited. This may give the implication that Mg alloying will not play that important a role as we formerly envisage for the fabrication of nano twins in UFG aluminium alloys. Thereby, this limited role in enhancing twinnability of Mg solutes can serve to explain the fact that twinning has been difficult to achieve and has been scarcely reported in previous papers on Al-Mg alloys, even when subjected to various SPD techniques like ECAP [1, 2, 61], HPT [3], and DPD [5].

5. Conclusion

In the present work, GPFE curves of face-centered cubic Al were calculated using first-principles calculations based on the slab shear methodology. A systematic analysis of the competition between different microscopic plastic deformation regimes (including twinning, stacking fault, and full slip) of Al in comparison to Cu was conducted based on the calculated GPFE curves.

With the aim to investigate the twinnability and variation of the intrinsic stacking fault energy γ_{ISFE} of Al-Mg alloys subjected to plastic deformation, a systematic investigation of the effect of Mg impurities upon the GPFE curve of Al was conducted with the aid of first-principles calculations. An activated Suzuki segregation behavior was established for the interactions between Mg solutes and stacking faults in Al, either intrinsic or extrinsic. Consistent with the previous experimental and theoretical reports, Mg solutes was found to decrease the γ_{ISFE} of Al. However, we've demonstrated that this decreasing effect is not so significant as that determined in experiments or theoretical predictions, and does not increase monotonically along with increasing Mg content. Furthermore, the effect of Mg alloying on deformation twinning in Al depends on the local concentration and configuration of Mg atoms around the deformation plane. Some specific distributions of Mg solutes near the deformation plane enhance the twinnability of Al, but the enhancement is limited. To sum up, Mg alloying is predicted in the present work as not so effective in the stacking fault energy (SFE)

engineering of Al alloys and a substantial increase of twinning propensity of Al via Mg alloying cannot be expected.

Acknowledgements

This work is financially supported under the FRINATEK project 'BENTMAT' (project number 222173) from Research Council of Norway. Computation time from the NOTUR consortium is gratefully acknowledged.

References

[1] Zha M, Li Y, Mathiesen RH, Bjørge R, Roven HJ (2014) Achieve high ductility and strength in an Al–Mg alloy by severe plastic deformation combined with inter-pass annealing. Mater Sci Eng A 598:141

[2] Zha M, Li Y, Mathiesen RH, Bjørge R, Roven HJ (2015) Microstructure evolution and mechanical behavior of a binary Al–7Mg alloy processed by equal-channel angular pressing. Acta Mater 84:42

[3] Sauvage X, Enikeev N, Valiev R, Nasedkina Y, Murashkin M (2014) Atomic-scale analysis of the segregation and precipitation mechanisms in a severely deformed Al–Mg alloy. Acta Mater 72:125

[4] Edalati K, Akama D, Nishio A, Lee S, Yonenaga Y, Cubero-Sesin JM, Horita Z (2014) Influence of dislocation–solute atom interactions and stacking fault energy on grain size of single-phase alloys after severe plastic deformation using high-pressure torsion. Acta Mater 69:68

[5] Jin S, Tao N, Marthinsen K, Li Y (2015) Deformation of an Al–7Mg alloy with extensive structural micro-segregations during dynamic plastic deformation. Mater Sci Eng A 628:160

[6] Lu K, Lu L, Suresh S (2009) Strengthening Materials by Engineering Coherent Internal Boundaries at the Nanoscale. Science 324:349

[7] Lu L, Chen X, Huang X, Lu K (2009) Revealing the Maximum Strength in Nanotwinned Copper. Science 323:607

[8] Muzyk M, Pakiela Z, Kurzydlowski KJ (2011) Ab initio calculations of the generalized stacking fault energy in aluminium alloys. Scr Mater 64:916

[9] Schulthess TC, Turchi PEA, Gonis A, Nieh TG (1998) Systematic study of stacking fault energies of random Al-based alloys. Acta mater 46:2215

[10] Morishige T, Hirata T, Uesugi T, Takigawa Y, Tsujikawa M, Higashi K (2011) Effect of Mg content on the minimum grain size of Al–Mg alloys obtained by friction stir processing. Scr Mater 64:355

[11] Bay B, Hansen N, Hughes DA, Kuhlmann-Wilsdorp D (1992) Evolution of f.c.c deformation structures in polyslip. Acta Metall Mater 40:205

[12] Hughes DA (1993) Microstructural evolution in a non-cell forming metal: Al-Mg. Acta Metall Mater 41:1421

[13] Jin SB, Zhang K, Bjørge R, Tao NR, Marthinsen K, Lu K, Li YJ (2015) Formation of incoherent deformation twin boundaries in a coarse-grained Al-7Mg alloy. Appl Phys Lett 107:091901

[14] Gray GT (1988) Deformation twinning in Al-4.8 wt% Mg. Acta metall 36:1745

[15] Shang SL, Wang WY, Zhou BC, Wang Y, Darling KA, Kecskes LJ, Mathaudhu SN, Liu ZK (2014) Generalized stacking fault energy, ideal strength and twinnability of dilute Mg-based alloys: A first-principles study of shear deformation. Acta Mater 67:168

[16] Zhang B, Wu L, Wan B, Zhang J, Li Z, Gou H (2015) Structural evolution, mechanical properties, and electronic structure of Al–Mg–Si compounds from first principles. J Mater Sci 50:6498

[17] Mohri T (2015) First-principles calculations of stability and phase equilibria in the Fe–Ni system. J Mater Sci 50:7705

[18] Vítek V (1968) Intrinsic stacking faults in body-centred cubic crystals. Phil Mag 18:773

[19] Siegel DJ (2005) Generalized stacking fault energies, ductilities, and twinnabilities of Ni and selected Ni alloys. Appl Phys Lett 87:121901

[20] Swygenhoven HV, Derlet PM, Frøseth AG (2004) Stacking fault energies and slip in nanocrystalline metals. Nature Mater 3:399

[21] Hartford J, von Sydow B, Wahnstrm G, Lundqvist BI (1998) Peierls barriers and stresses for edge dislocations in Pd and Al calculated from first principles. Phys Rev B 58:2487

[22] Lu G, Kioussis N, Bulatov VV, Kaxiras E (2000) Generalized-stacking-fault energy surface and dislocation properties of aluminum. Phys Rev B 62:3099

[23] Ogata S, Li J, Yip S (2002) Ideal Pure Shear Strength of Aluminum and Copper. Science 298:807

[24] Liu XY, Ercolessi F, Adams JB (2004) Aluminium interatomic potential from density functional theory calculations with improved stacking fault energy. Model Simul Mater Sci Eng 12:665

[25] Finkenstadt D, Johnson DD (2006) Solute/defect-mediated pathway for rapid nanoprecipitation in solid solutions: gamma surface analysis in fcc Al-Ag. Phys Rev B 73:024101

[26] Kibey S, Liu JB, Johnson DD, Sehitoglu H (2007) Predicting twinning stress in fcc metals: Linking twin-energy pathways to twin nucleation. Acta Mater 55:6843

[27] Qi Y, Mishra RK (2007) Ab initio study of the effect of solute atoms on the stacking fault energy in aluminum. Phys Rev B 75: 224105

[28] Woodward C, Trinkle DR, Hector JLG, Olmsted DL (2008) Prediction of Dislocation Cores in Aluminum from Density Functional Theory. Phys Rev Lett 100:045507

[29] Jahnátek M, Hafner J, Krajčí M (2009) Shear deformation, ideal strength, and stacking fault formation of fcc metals: A density-functional study of Al and Cu. Phys Rev B 79:224103

[30] Wu X, Wang R, Wang S (2010) Generalized-stacking-fault energy and surface properties for HCP metals: A first-principles study. Appl Surf Sci 256:3409

[31] Jin ZH, Dunham ST, Gleiter H, Hahn H, Gumbsch P (2011) A universal scaling of planar fault energy barriers in face-centered cubic metals. Scr Mater 64:605.

[32] Branicio PS, Zhang JY, Srolovitz DJ (2013) Effect of strain on the stacking fault energy of copper: A first-principles study. Phys Rev B 88: 064104

[33] Asadi E, Zaeem MA, Moitra A, Tschopp MA (2014) Effect of vacancy defects on generalized stacking fault energy of fcc metals. J Phys: Condens Matter 26:115404

[34] Bhogra M, Ramamurty U, Waghmare UV (2014) Temperature-dependent stability of stacking faults in Al, Cu and Ni: first-principles analysis. J Phys: Condens Matter 26:385402

[35] Wu XZ, Liu LL, Wang R, Liu Q (2014) The generalized planar fault energy, ductility, and twinnability of Al and Al–X (X = Sc, Y, Dy, Tb, Nd) at different temperatures: Al and Al–X(X = Sc, Y, Dy, Tb, Nd) at different temperatures: A first-principles study. Chin Phys B 23:066104

[36] Hunter A, Beyerlein IJ (2015) Relationship between monolayer stacking faults and twins in nanocrystals. Acta Mater 88:207.

[37] Kibey S, Liu JB, Johnson DD, Sehitoglu H (2006) Generalized planar fault energies and twinning in Cu-Al alloys. Appl Phys Lett 89: 191911

[38] Jo M, Koo YM, Lee BJ, Johansson B, Vitos L, Kwon SK (2014) Theory for plasticity of face-centered cubic metals. PNAS 111:6560

[39] Kresse G, Furthmiiller J (1996) Efficiency of ab-initio total energy calculations for metals and semiconductors using a plane-wave basis set. Comp Mater Sci 6:15

[40] Kresse G, Furthmüller J (1996) Efficient iterative schemes for ab initio total-energy calculations using a plane-wave basis set. Phys Rev B 54:11169

[41] P.E. Blöchl (1994) Projector augmented-wave method. Phys Rev B 50:17953

[42] Kresse G, Joubert D (1999) From ultrasoft pseudopotentials to the projector augmented-wave method. Phys Rev B 59:1758

[43] Perdew JP, Burke K, Ernzerhof M (1996) Generalized Gradient Approximation Made Simple. Phys Rev Lett 77:3865

[44] Monkhorst HJ, Pack JD (1976) Special points for Brillouin-zone integrations. Phys Rev B 13:5188

[45] Blöchl PE, Jepsen O, Andersen OK (1994) Improved tetrahedron method for Brillouin-zone integrations. Phys Rev B 49:16223

[46] Zhao Q, Holmedal B, Li YJ, Sagvolden E, Løvvik O (2015) Multi-component solid solution and cluster hardening of Al–Mn–Si alloys. Mater Sci Eng A 625:153

[47] Wang C, Wang H, Zhang H, Nan X, Xue E, Jiang Q (2013) First-principles study of generalized-stacking-fault (GSF) energy in Mg with Al and Zn alloyings. J Alloys Comp 575:423

[48] Shang SL, Zacherl CL, Fang HZ, Wang Y, Du Y, Liu ZK (2012) Effects of alloying element and temperature on the stacking fault energies of dilute Ni-base superalloys. J Phys: Condens Matter 24: 505403

[49] Mehl MJ, Papaconstantopoulos DA, Kioussis N, Herbranson M (2000) Tight-binding study of stacking fault energies and the Rice criterion of ductility in the fcc metals. Phys Rev B 61:4894

[50] Cotterill RMJ, Doyama M (1966) Energy and Atomic Configuration of Complete and Dissociated Dislocations. I. Edge Dislocation in an fcc Metal*. Phys Rev 145:465

[51] Rice JR (1992) Dislocation nucleation from a crack tip an analysis based on the peierls concept. J Mech Phys Solids 40:239

[52] Tadmor EB, Hai S (2003). A Peierls criterion for the onset of deformation twinning at a crack tip. J Mech Phys Solids 51:765

[53] Tadmor EB, Bernstein N (2004) A first-principles measure for the twinnability of FCC metals. J Mech Phys Solids 52:2507

[54] Bernstein N, Tadmor EB (2004) Tight-binding calculations of stacking energies and twinnability in fcc metals. Phys Rev B 69:094116

[55] Soliman MS (1993) The high-temperature creep behaviour of an Al-1 wt% Cu solid-solution alloy. J Mater Sci 28:4483

[56] Hammer B, Jacobsen KW, Milman V, Payne MC (1992) Stacking fault energy in aluminium. J Phys: Condens Matter 4:10453

[57] Fan T, Wei L, Tang B, Peng L, Ding W (2014) Effect of temperature-induced solute distribution on stacking fault energy in Mg–X(X = Li, Cu, Zn, Al, Y and Zr) solid solution: a first-principles study. Phil Mag 94:1578

[58] Dontsova E, Rottler J, Sinclair CW (2014) Solute-defect interactions in Al-Mg alloys from diffusive variational Gaussian calculations. Phys Rev B 90:174102

[59] Løvvik OM, Sagvolden E, Li YJ (2014) Prediction of solute diffusivity in Al assisted by first principles molecular dynamics. J Phys: Condens Matter 26:025403

[60] Kritzinger S, Dobson PS, Smallman RE (1967) The influence of a dilute magnesium addition on the growth ant shrinkage of dislocation loops in aluminium. Phil Mag 16:217

[61] Morris DG, Munoz-Morris MA (2002) Microstructure of severely deformed Al–3Mg and its evolution during annealing. Acta Mater 50:4047

[62] Murr LE (1975) Interfacial Phenomena in Metals and Alloys. Addison Wesley, Reading, MA.

[63] Smallman RE, Dobson PS (1970) Stacking Fault Energy Measurement from Diffusion. Metall Trans 1:2383

[64] Mills MJ, Stadelmann P (1989) A study of the structure of Lomer and 600 dislocations in Al using high-resolution transmission electron microscopy. Philos Mag A 60:355

[65] Dillamore IL, Smallman RE (1965) The stacking-fault energy of F.C.C. metals. Philos Mag 12:191

[66] Brandl C, Derlet PM, Swygenhoven HV (2007) General-stacking-fault energies in highly strained metallic environments: Ab initio calculations. Phys Rev B 76:054124

[67] Zimmerman JA, Gao H, Abraham FF (2000) Generalized stacking fault energies for embedded atom FCC metals. Modelling Simul Mater Sci Eng 8:103

[68] Denteneer PJH, Sole JM (1991) Defect energetics in aluminium. J Phys: Condms Matter 3:8777

[69] Kioussis N, Herbranson M, Collins E, Eberhart ME (2002) Topology of Electronic Charge Density and Energetics of Planar Faults in fcc Metals. Phys Rev Lett 88:125501

[70] Wright AF, Daw MS, Fong CY (1992) Theoretical investigation of (111) stacking faults in aluminium. Philos Mag A 66:387

[71] Simon JP (1979) A review of twin and stacking fault energies in Al, Mg and Be. J Phys F: Metal Phys 9:425

[72] Devlin JF, Bollmann W (1975) A Rapid Calculational Technique for the Stacking-Fault Problem. Phys Status Solidi A 27:K57

[73] Jin Q, Wang P, Ding D (1993) ASW first principles calculation of the intrinsic and extrinsic stacking fault energies in aluminium. Phys Lett A 174:437

[74] Wei XM, Zhang JM, Xu KW, Ji V (2008) Surface effect on the GSF energy of Al. Appl Surf Sci 254:6683

[75] Mishin Y, Farkas D, Mehl MJ, Papaconstantopoulos DA (1999) Interatomic potentials for monoatomic metals from experimental data and ab initio calculations. Phys Rev B 59:3393

[76] Crampin S, Hampel K, Vvedensky DD, MacLaren JM (1990) The calculation of stacking fault energies in close-packed metals. J Mater Res 5:2107

[77] Wilkes P, Sargent CM (1972) A Calculation of the Stacking-Fault and Twin Energies for Aluminium. Met Sci J 6:216

[78] Fullman RL. Interfacial Free Energy of Coherent Twin Boundaries in Copper (1951) J Appl Phys 22:448

[79] Howie A, Swann PR (1961) Direct measurements of stacking-fault energies from observations of dislocation nodes. Phil Mag 6:1215

[80] Peissker VE (1965) Critical stress for cross slip and stacking fault energies of copper base mixed crystals. Acta Metall 13:419

[81] Stobbs WM, Sworn CH (1971) The weak beam technique as applied to the determination of the stacking-fault energy of copper. Phil Mag 24:1365

[82] Carter CB, Ray ILF (1977) On the stacking-fault energies of copper alloys. Phil Mag 35:189

[83] Thornton PR, Mitchell TE (1962) Deformation twinning in alloys at low temperatures. Phil Mag 7:361

[84] Schweizer S, Elsasser C, Hummler K, Fahnle M (1992) Ab initio calculation of stacking-fault energies in noble metals. Phys Rev B 46:14270

[85] Wang LG, Šob M (1999) Structural stability of higher-energy phases and its relation to the atomic configurations of extended defects: The example of Cu. Phys Rev B 60:844

[86] Heino P (1999) Stacking-fault energy of copper from molecular-dynamics simulations. Phys Rev B 60:14625

[87] Rosengaard NM, Skriver HL (1993) Calculated stacking-fault energies of elemental metals. Phys Rev B 47:12865

Tables

Table 1. Binding energy (meV) for different Mg-Mg pairs at different neighboring distance in the Al matrix. A positive value indicates a favorable binding state. The possible occupations of Mg solutes in the Al matrix are as indicated in Fig. 1(a).

Occupations	Neighbors	Mg-Mg
1-2	1nn	-15.9
1-3	1nn'	-13.1
1-4	2nn	27.1

1-5	2nn'	14.6
1-6	3nn	7.0
1-7	3nn'	3.7
1-8	4nn	21.0
1-9	4nn'	13.9
1-10	5nn	0.6

Table 2. Calculated values of the unstable stacking fault energy γ_{USFE}, intrinsic stacking fault energy γ_{ISFE}, unstable twinning fault energy γ_{UTFE} and twinning fault energy γ_{TFE} of Al, in comparison with previous theoretical and experimental results. The energies are in mJ/m^2.

γ_{USFE}	γ_{ISFE}	γ_{UTFE}	γ_{TFE}	$\gamma_{ISFE}/\gamma_{USFE}$	$\gamma_{UTFE}/\gamma_{USFE}$	$\gamma_{UTFE}-\gamma_{USFE}$	τ_a (Twinnability)	Method and approach		Reference
177.4	142.4	226.5	135.4	0.803	1.277	49.1	0.898	First-principles (FP)	PAW-GGA-PBE	Present work
-	166.0	-	-	-	-	-	-	Experiment (Exp.)	-	[62]
-	135.0	-	-	-	-	-	-	Exp.	Annealing Kinetics of Dislocation Loops	[63]
-	150.0	-	-	-	-	-	-	Exp.	High-resolution transmission electron microscopy	[64]
-	200.0	-	-	-	-	-	-	Exp.	Dimensions of Stacking-Fault Tetrahedra	[65]
177.0	140.2	-	-	0.792	-	-	-	FP	PAW-GGA-PBE	[36]
177.0	143.0	-	147.0	0.808	-	-	-	FP	PAW-LDA	[21]
174.0	149.0	-	152.0	0.856	-	-	-	FP	PAW-LDA	[25]
-	142.0	-	-	-	-	-	-	FP	PAW-GGA-PW91	[27]
178.0	146.0	-	-	0.820	-	-	-	FP	PAW-GGA-PW91	[66]
175.0	158.0	-	-	0.903	-	-	-	FP	PAW-GGA-PW91	[23]
162.0	130.0	215.0	113.0	0.802	1.327	53.0	0.881	FP	PAW-GGA-PW91	[26]
-	122.0	-	-	-	-	-	-	FP	PAW-GGA	[28]
-	134.0	-	-	-	-	-	-	FP	US-LDA	[28]
-	124.0	-	-	-	-	-	-	FP	US-GGA	[28]
224.0	164.0	-	-	0.732	-	-	-	FP	US-LDA	[22]
-	156.0	-	138.0	-	-	-	-	FP	US-LDA	[56]
169.0	134.0	-	-	0.793	-	-	-	FP	PAW-GGA-PBE + Simple alias shear	[29]
169.0	126.0	-	-	0.746	-	-	-	FP	PAW-GGA-PBE + Pure alias shear	[29]
-	151.0	-	-	-	-	-	-	FP	PAW-LDA	[21]
-	161.0	-	-	-	-	-	-	FP	PAW-LDA	[21]
225.0	158.0	-	-	0.702	-	-	-	FP	PAW-GGA-PW91	[30]
189.1	162.4	238.6	-	0.859	1.262	49.5	0.896	FP	PAW-GGA-PBE	[8]
140.0	112.0	196.0	-	0.800	1.400	56.0	0.858	FP	PAW-GGA-PBE	[31]
171.5	164.2	-	-	0.957	-	-	-	FP	PAW-GGA-PBE	[33]
197.0	162.0	-	-	0.822	-	-	-	FP	PAW-GGA-PBE	[34]
185.0	142.0	236.0	-	0.768	1.276	51.0	0.903	FP	PAW-GGA-PBE	[35]
213.0	153.0	-	-	0.718	-	-	-	FP	PAW-LDA	[67]
-	126.0	-	108.0	-	-	-	-	FP	Augmented Plane Wave	[68]
215.0	170.0	-	-	0.791	-	-	-	FP	Full-Potential Linear Muffin Tin Orbital (FP-LMTO)	[69]

-	164.0	-	-	-	-	-	-	FP	FP-LMTO	[49]
-	161.0	-	151.0	-	-	-	-	FP	Kohn-Sham fucntions	[70]
-	160.0	-	-	-	-	-	-	FP	Pseudopotential theory	[71]
-	142.0	-	-	-	-	-	-	FP	Pseudopotential theory	[72]
-	96.0	-	-	-	-	-	-		Tight binding	[49]
-	154.0	-	138.0	-	-	-	-		Augmented Spherical Wave	[73]
151.3	146.0	200.0	-	0.965	1.322	48.7	0.861		Molecular Dynamics Simulation	[20]
123.9	95.4	149.7	-	0.770	1.208	25.8	0.928		Molecular Dynamics Simulation	[20]
238.0	142.2	-	-	0.597	-	-	-		Second-Nearest-Neighbor Modified Embedded Atom Method	[74]
-	128.0	-	-	-	-	-	-		Embedded Atom Method (EAM)	[24]
168.0	146.0	-	-	0.869	-	-	-		EAM	[75]
168.6	147.0	-	-	0.872	-	-	-		EAM	[33]
220.5	127.4	-	-	0.578	-	-	-		EAM	[33]
287.2	145.4	-	-	0.506	-	-	-		Modified Embedded Atom Method	[33]
-	124.0	-	118.0	-	-	-	-		Layer–Korringer–Kohn–Rostoker method	[76]
-	140.0	-	130	-	-	-	-		Pair Potential	[77]

Table 3. Calculated values of the unstable stacking fault energy γ_{USFE}, intrinsic stacking fault energy γ_{ISFE}, unstable twinning fault energy γ_{UTFE} and twinning fault energy γ_{TFE} of Cu, in comparison with previous theoretical and experimental results. The energies are in mJ/m^2.

γ_{USFE}	γ_{ISFE}	γ_{UTFE}	γ_{TFE}	$\gamma_{ISFE}/\gamma_{USFE}$	$\gamma_{UTFE}/\gamma_{USFE}$	γ_{UTFE}-γ_{USFE}	τ_a (Twinnability)	Method and approach		Reference
161.5	40.5	181.4	42.4	0.251	1.123	19.9	1.036	First-principles (FP)	PAW-GGA-PBE	Present Work
-	42.0	-	-	-	-	-	-	Experiment (Exp.)	Annealing Kinetics of Dislocation Loops	[78]
-	40.0	-	-	-	-	-	-	Exp.	Transmission Electron Microscopy	[79]
-	50.0	-	-	-	-	-	-	Exp.	Seeger relation on τ_{111}	[80]
-	41.0	-	-	-	-	-	-	Exp.	Weak Beam Technique	[81]
-	45.0	-	-	-	-	-	-	Exp.	Weak Beam Technique	[82]
-	78.0	-	-	-	-	-	-	Exp.	-	[62]
-	35-45	-	-	-	-	-	-	Exp.	-	[83]
163.7	38.5	-	-	0.235	-	-	-	FP	PAW-GGA-PBE	[36]
181.0	41.0	200.0	40.0	0.227	1.105	19.0	1.048	FP	PAW-GGA-PW91	[37]
158.0	36.0	179.0	-	0.228	1.133	21.0	1.035	FP	PAW-GGA-PBE	[31]
-	33.0	-	-	-	-	-	-	FP	PAW-GGA-PW91	[27]
158.0	39.0	-	-	0.247	-	-	-	FP	PAW-GGA-PW91	[23]
164.0	38.0	-	-	0.232	-	-	-	FP	PAW-GGA-PW91	[66]
180.0	41.0	-	-	0.228	-	-	-	FP	PAW-GGA-PBE + Simple alias shear	[29]
186.0	37.0	-	-	-	-	-	-	FP	PAW-GGA-PBE + Pure alias shear	[29]
-	51.0	-	54.0	-	-	-	-	FP	PAW-LDA	[21]
-	53.0	-	-	-	-	-	-	FP	PAW-LDA	[21]
-	41.0	-	-	-	-	-	-	FP	PAW-GGA-PBE	[32]
163.0	41.3	-	-	0.253	-	-	-	FP	PAW-GGA-PBE	[33]
149.0	42.0	-	-	0.282	-	-	-	FP	PAW-GGA-PBE	[34]
175.0	43.0	-	-	0.246	-	-	-	FP	PAW-GGA-PW91	[30]
210.0	49.0	-	-	0.233	-	-	-	FP	PAW-LDA	[67]
-	50.0	-	-	-	-	-	-	FP	PAW-LDA	[84]
-	64.0	-	-	-	-	-	-	FP	Full-Potential	[85]
154.1	20.6	163.3	-	0.134	1.060	9.2	1.084	Molecular Dynamics Simulation		[20]
173.1	33.5	190.0	-	0.194	1.098	16.9	1.056	Molecular Dynamics Simulation		[20]
162.6	44.4	-	-	0.273	-	-	-	Embedded Atom Method (EAM)		[33]
234.0	44.1	-	-	0.188	-	-	-	EAM		[33]
247.2	72.2	-	-	0.292	-	-	-	Modified Embedded Atom Method		[33]

-	30.0	-	-	-	-	-	-	Morse Potential	[50]
-	78.0	-	-	-	-	-	-	Effective Medium Theory (EMT) and Embedded Atom Model (EAM) potential	[86]
-	56.0	-	-	-	-	-	-	Tight Binding Linear Muffin Tin Orbital Green's Function	[87]

Table 4. The effect of Mg concentration on the unstable stacking fault energy γ_{USFE}, intrinsic stacking fault energy γ_{ISFE}, unstable twinning fault energy γ_{UTFE} and twinning fault energy γ_{TFE} of Al. The energies are in mJ/m^2. The subscript numbers in the "Occupation" column correspond to the atomic positions as defined in Fig. 1(c) for different Mg substitutions.

System	Mg concentration, at. %	Occupation	γ_{USFE}	γ_{ISFE}	γ_{UTFE}	$2\gamma_{TFE}$	$\gamma_{ISFE}/\gamma_{USFE}$	$\gamma_{UTFE}/\gamma_{USFE}$	γ_{UTFE}-γ_{USFE}	τ_a (Twinnability)
Al_{96}	0	-	177.4	142.4	226.5	135.4	0.803	1.277	49.1	0.898
$Al_{95}Mg_1$	1.08	$Mg_{(1)}$	168.0	135.0	211.6	119.1	0.804	1.260	43.6	0.904
$Al_{94}Mg_2$	2.16	$Mg_{(1,4)}$	162.7	130.9	202.2	108.3	0.805	1.243	39.5	0.910
$Al_{93}Mg_3$-1	3.13	$Mg_{(1,10,12)}$	167.0	133.9	203.9	103.7	0.802	1.221	36.9	0.919
$Al_{93}Mg_3$-2	3.13	$Mg_{(1,9,11)}$	163.5	133.6	202.8	104.8	0.817	1.241	39.4	0.909
$Al_{93}Mg_3$-3	3.13	$Mg_{(1,6,8)}$	156.5	132.1	213.9	142.9	0.844	1.367	57.4	0.863
$Al_{93}Mg_3$-4	3.13	$Mg_{(1,5,7)}$	156.3	128.4	208.7	130.3	0.822	1.335	52.4	0.876
$Al_{92}Mg_4$-1	4.17	$Mg_{(1,4,5,7)}$	154.7	133.9	212.7	142.4	0.866	1.375	58.1	0.857
$Al_{92}Mg_4$-2	4.17	$Mg_{(1,4,9,11)}$	164.6	134.4	201.3	101.9	0.816	1.223	36.7	0.916
$Al_{90}Mg_6$-1	6.28	$Mg_{(1,4,5,6,7,8)}$	163.2	145.5	233.6	179.9	0.891	1.432	70.5	0.837
$Al_{90}Mg_6$-2	6.28	$Mg_{(1,4,9,10,11,12)}$	169.3	141.0	210.7	105.3	0.833	1.244	41.4	0.906
$Al_{90}Mg_6$-3	6.28	$Mg_{(1,4,5,7,10,12)}$	158.8	133.9	212.3	133.1	0.843	1.338	53.5	0.872
$Al_{90}Mg_6$-4	6.28	$Mg_{(1,4,5,7,9,11)}$	151.6	131.8	208.4	132.1	0.870	1.374	56.8	0.870

Figures.

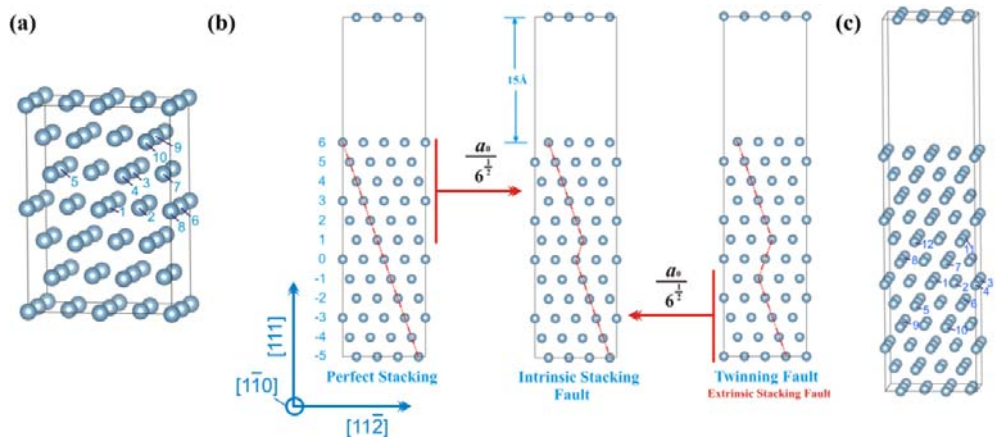

Fig 1. (a) Identification of the Al sites for substitution of Mg solutes. (b) Typical slab atomic configurations adopted in the present calculations including the perfect stacking, intrinsic stacking fault, and twinning fault configurations. A 15 Å thick vacuum layer was included in all the slab models. The displacement path of the GPFE along the $<11\bar{2}>$ direction is also illustrated. (c) Atomic positions (indicated as 1-12) for possible Mg solute substitutional sites to evaluate its effect on the GPFE of Al.

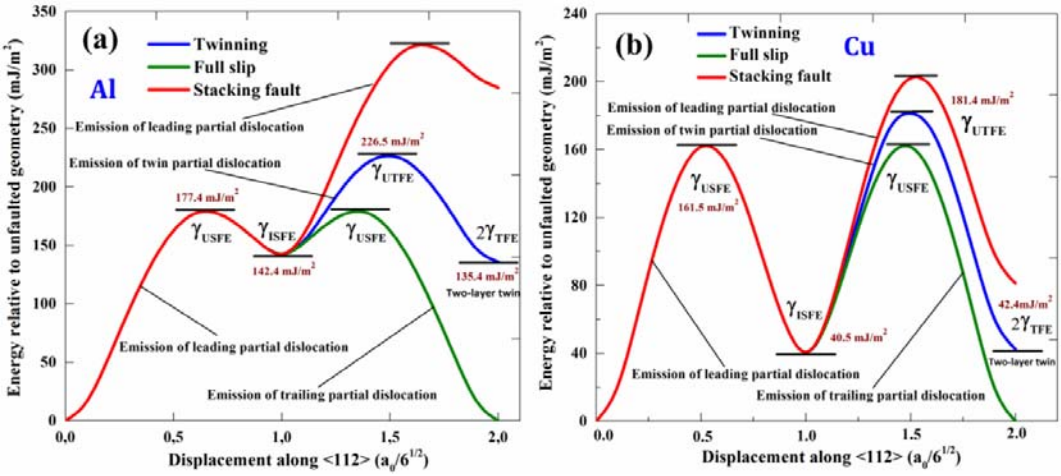

Fig 2. Generalized planar fault energy (GPFE) curves for (a) Al and (b) Cu.

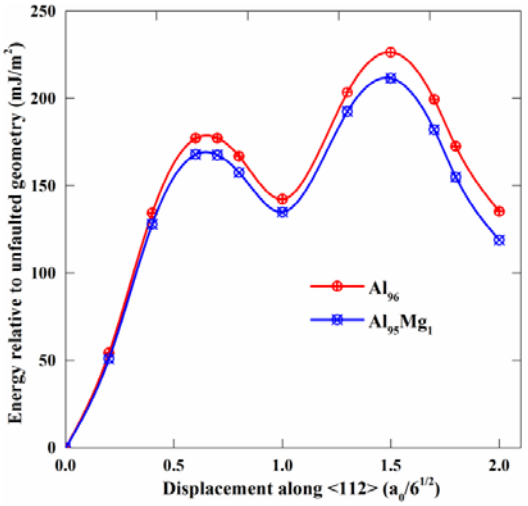

Fig 3. The effect of a single substitutional Mg solute on the GPFE curves of Al. The Mg solute is placed in the stacking fault plane.

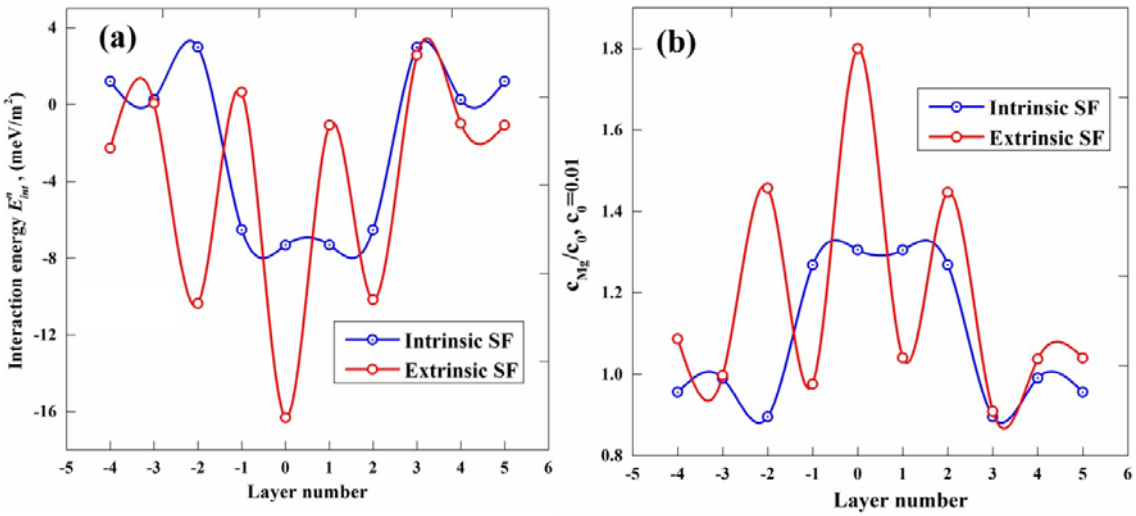

Fig 4. (a) Layer-by-layer interaction energy of a single Mg solute with intrinsic and extrinsic stacking faults in Al. (b) Spatial concentration profile of Mg in the vicinity of intrinsic and extrinsic stacking faults in Al, , evaluated based on Eq. (7) at the nominal concentration of c_0=0.01, and temperature T=300K. Lines are only drawn as guides to the eye.

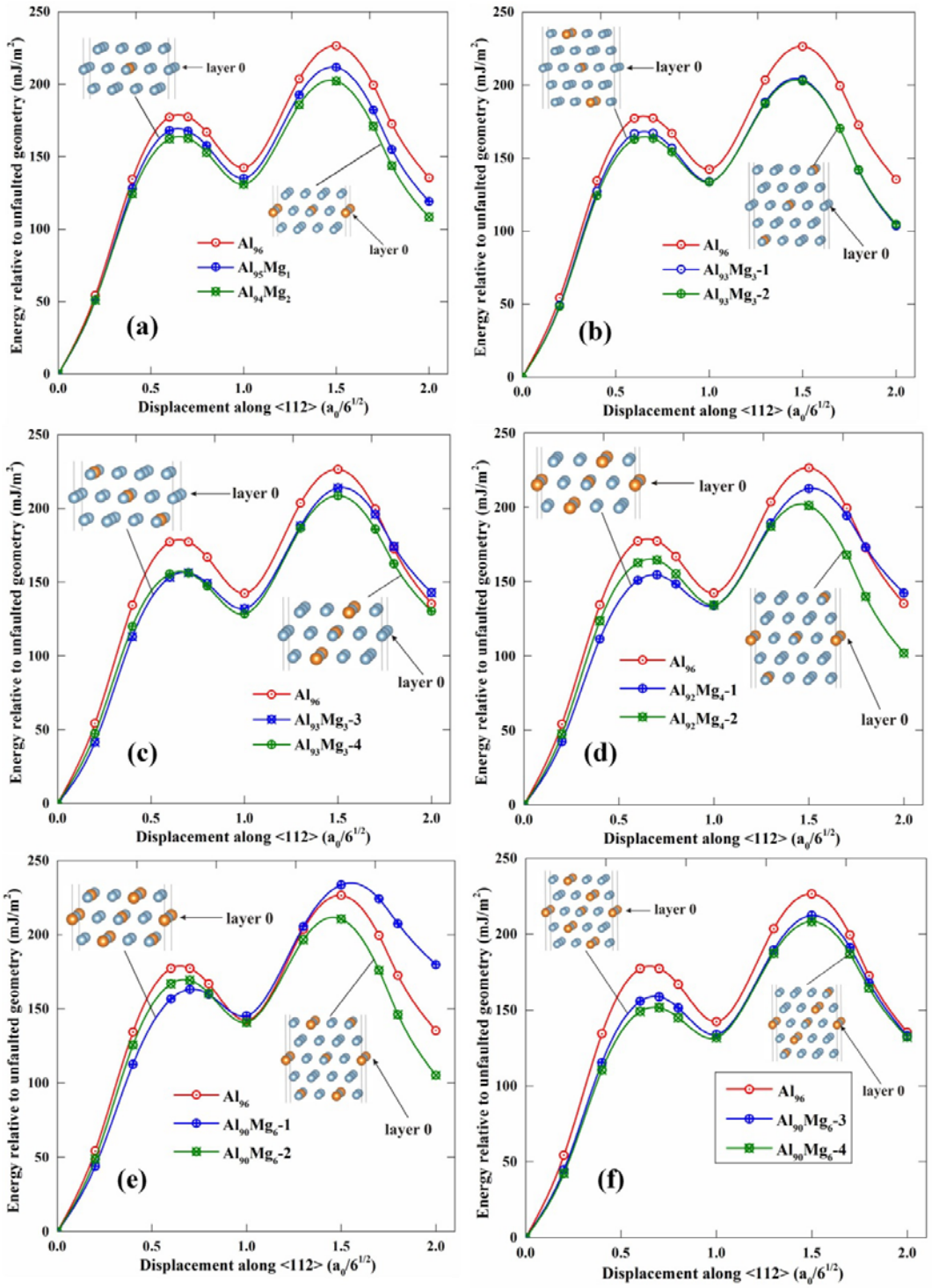

Fig 5. The effect of Mg concentration and configuration on the GPFE curves of Al. The Mg distributions at various concentrations near the fault plane in the perfect stacking configurations are as indicated. For a detailed description of the Mg configuration in all these models, please refer to Table 4.

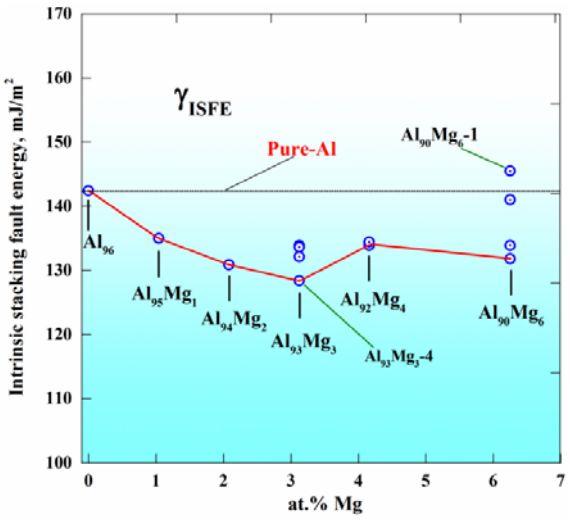

Fig 6. The calculated intrinsic stacking fault energy, γ_{ISFE}, as a function of the Mg concentration for Al_xMg_y models.

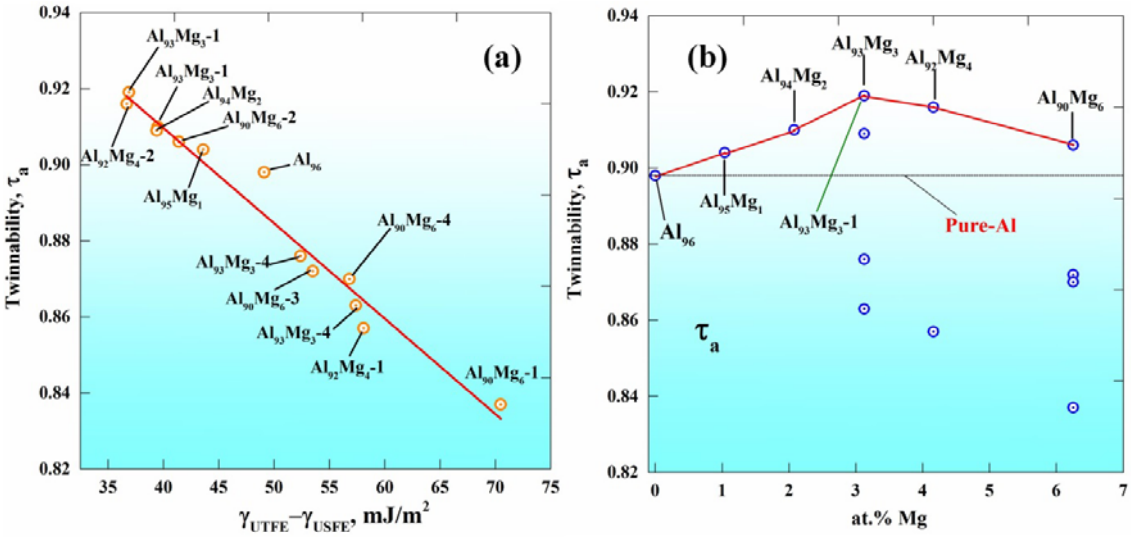

Fig 7. (a) The linear correlation between twinnability parameter τ_a and γ_{UTFE}-γ_{USFE} for Al_xMg_y, (b) the twinnability parameter τ_a of Al_xMg_y models as a function of Mg concentration.